*Pure Appl. Chem.*, Vol. 72, No. 11, pp. 2111–2126, 2000.
© 2000 IUPAC

# Development and application of very high temperature mass spectrometry. Vapor pressure determinations over liquid refractories*

J. W. Hastie†, D. W. Bonnell, and P. K. Schenck

*National Institute of Standards and Technology (NIST), Gaithersburg, Maryland 20899-8522, USA*

*Abstract*: Existing thermodynamic and vaporization data for liquid refractories are based either on estimates or on data extrapolated from studies on the solids obtained at much lower temperatures. Previously, we have shown that pulsed laser heating, coupled with time-dependent mass spectrometry of the free-expansion vapor plume, can be used for semi-quantitative measurements of vaporization thermochemistry. The present work extends this approach with the development of (a) more direct, and more accurate, methods for determining the system temperature and pressure; (b) improved experimental and theoretical determinations of key parameters such as ionization cross sections; and (c) improved characterization of the gas dynamic expansion and thermal equilibration processes. Example material systems considered include C, SiC, $Al_2O_3$, $ZrO_2$–7%$Y_2O_3$, and $Y_2O_3$ at temperatures and total pressures typically in the range of 3000 to 5000 K and 0.01 to 10 bar, respectively (1 bar = $10^5$ $Nm^{-2}$).

## INTRODUCTION

The thermodynamic properties of inorganic materials at very high temperatures, and hence at high vapor pressures, are often required for processing or performance assessment. Examples of current technologies include those based on plasma spray of liquid particles and on electron beam and laser vaporization of liquid pools. The long-standing need for more accurate thermochemical data for nuclear reactor materials at very high temperatures continues. In the present context, we consider very high temperatures to include the range 2500 to 5500 K. The lower limit corresponds, approximately, to the practical upper limit of classical high-temperature thermochemistry techniques, particularly Knudsen effusion mass spectrometry (KMS). The upper limit is somewhat arbitrary but allows for inclusion of refractory liquids at vapor pressures up to at least 10 bar and without thermal ionization as a major contributor to the vapor composition. For this temperature range, thermochemical data, including partial pressures, are generally based on an extrapolation of data obtained from studies at much lower temperatures or from estimation procedures. Thus, thermochemical data presented in critically evaluated thermochemical reference tables (JANAF [1], IVTANTHERMO [2]) have significant uncertainty, which could be even greater than expected in the very high temperature range.

Because of the impracticality of containing reactive liquids and vapors at temperatures much beyond 2500 K, an essentially containerless approach, developed earlier, has been used [3,4]. This approach utilizes short time-scale (~20 ns) laser pulses as a directed, spatially constrained heat source as discussed in earlier work (see refs. 4, 5, and cited literature). An additional measurement complexity arises from the propensity of high-temperature materials to vaporize as a mixture of complex and simple species, with the former often increasing in importance with temperature [6]. In order to speci-

*Lecture presented at the 10th International Conference on High Temperature Materials Chemistry (HTMC-X), Jülich, Germany, 10–14 April 2000. Other presentations are published in this issue, pp. 2101–2186.

†Corresponding author; U.S. Government contribution not subject to copyright.

fy the vapor molecular weight (e.g,. for use in mass transport–pressure relationships), the identity and relative concentrations of these species must first be established. Mass spectrometry (MS) is the most practical (if not the only) means of obtaining such information, and MS has been coupled with pulsed lasers to provide a technique we term laser vaporization mass spectrometry (LVMS). A distinction should be made between LVMS and other, nonthermal laser-MS coupled experiments such as laser microprobe mass analysis (LAMMA) and pulsed laser deposition (PLD) monitoring [7]. In these latter cases, highly nonthermal processes are present, and little or no thermochemical insight is usually gained under the higher laser powers utilized. Even for LVMS experiments, a serious high pressure limit arises from laser–vapor interaction, giving rise to nonthermal effects such as superheating, electronic excitation, and photo-dissociation. As these effects are readily identified, they can usually be avoided by adjusting the laser parameters of wavelength, fluence, and pulse width. Nonthermal modes of laser–solid (or liquid) interaction can also occur, particularly with shorter wavelengths, shorter pulses, or higher fluences.

The use of pulsed laser heating for vaporization thermochemistry studies has had a sporadic history over a period of about three decades. The early work of the groups of Ohse [8] and Olander [9] utilized relatively long pulse (~μs to ms) infrared lasers. A few non-mass spectrometric experiments were also carried out, e.g., by Covington *et al.* [10] and Tunney *et al.* [11]). In our laboratory, the technique was modified to include use of much shorter laser pulses [3]. Experimental difficulties and data accuracy limitations were present with each of these early studies. Accurate conversion of mass spectral ion intensities to partial pressures suffered from the need to measure, or calculate, gas dynamic factors not present in conventional KMS. In addition, the usual KMS limitations of electron impact fragmentation and unknown ionization cross-sections were also present. Temperature measurements were also difficult, relying on two-color pyrometry and assumed emissivity for longer pulse experiments and on indirect thermochemical and gas dynamic approaches for the short-pulse experiments. In the present study, these limitations have been overcome, and the accuracy of vapor pressure data is typically at least an order-of-magnitude better than the extrapolated/estimated literature data.

Olander recently reviewed and compared the general features of short- and long-pulse laser materials interaction for thermal vaporization measurements [9]. Advantages and disadvantages exist with each case. With the latter, a practical upper limit vapor density occurs with the onset of expansion nucleation and clustering. This onset is apparently very material-specific and can occur at pressures as low as ~$10^{-4}$ bar for the case of $UO_2$. A similar restriction was found for $ZrO_2$ [9]. With the former short-pulse case, nonthermal interactions are more likely. However, these can usually be avoided or minimized for select conditions of laser wavelength, and for fluences not too far above the vaporization threshold. Also, no evidence has yet been found for a cluster-forming limitation, and total vapor pressures typically in the range ~0.01 bar to ~10 bar have been measured in the present study. This pressure range is characteristic for vaporization of liquid refractories, whereas at temperatures corresponding to pressures of $10^{-4}$ bar, such materials are usually solids. Hence, short-pulse lasers are the most appropriate choice for thermodynamic studies of liquid refractories or other materials at temperatures where vapor pressures are of the order of 1 bar. However, the short time-scale (typically 5 to 30 ns) associated with these lasers significantly increases the experimental difficulties, particularly the direct measurement of temperature. Also, the hydrodynamic nature of the pre-sampling vapor expansion process necessitates the use of special calibration procedures to convert mass spectral signals, or alternatively, deposition rates, to partial and total pressures. The necessity of demonstrating thermal vaporization on a case by case basis is also a special requirement of the present LVMS technique. In the current study, we have measured species partial and total pressures for several of the more well-established systems (i.e., C and $Al_2O_3$), in order to test the reliability of the lower temperature data and of the extrapolation procedures. Measurements have also been made on less well-established systems (i.e., SiC, $Y_2O_3$, and $ZrO_2$–7%$Y_2O_3$). These particular systems are present as high vapor pressure liquids in industrial physical vapor deposition and thermal spray processes. The SiC system, unlike C and $Al_2O_3$, may not vaporize congruently and melts by disproportionation to Si($\ell$) and C(s,solution) [12]. This

vaporization mode provides an additional test of the LVMS technique, where congruent vaporization can occur under nonthermal ablation conditions, such as are used for PLD; observation of noncongruent behavior would then be more consistent with a thermal rather than ablative process. Also, the presence of a Si($\ell$) phase allows one to use the well-established pressure data for Si($\ell$) to test the reliability of the LVMS measured pressures of Si and $Si_2$.

## APPARATUS

In our earlier studies we described the basic apparatus used for short-pulse LVMS [4]. A schematic of this apparatus, including various modifications made for the present work, is given in Fig 1. The essential features of this apparatus are:

- high-power pulsed laser sources, with optics to control the beam diameter and angle of attack at the target surface. Lasers used include: (a) Nd:YAG, with wavelengths of 1064 nm and 532 nm; and (b) excimer at 248 nm. Other wavelengths available with these lasers were not used for these studies. Pulse widths were typically ~20 ns (Nd:YAG) and 10 ns (excimer).
- computer-controlled target-support x-y stage. The high-speed motion of the stage was programmed to assure a fresh target area was used with successive laser pulses. The stage could also be tilted *in situ* when necessary.
- deposition rate monitor, positioned 3 cm from target at $\theta = 0°$ and with remote positioning control to allow removal from the beam axis during MS detection and for angular distribution ($\cos^n \theta$, where $n \geq 1$) measurements. The rate and MS measurements are made sequentially, under essentially identical conditions.

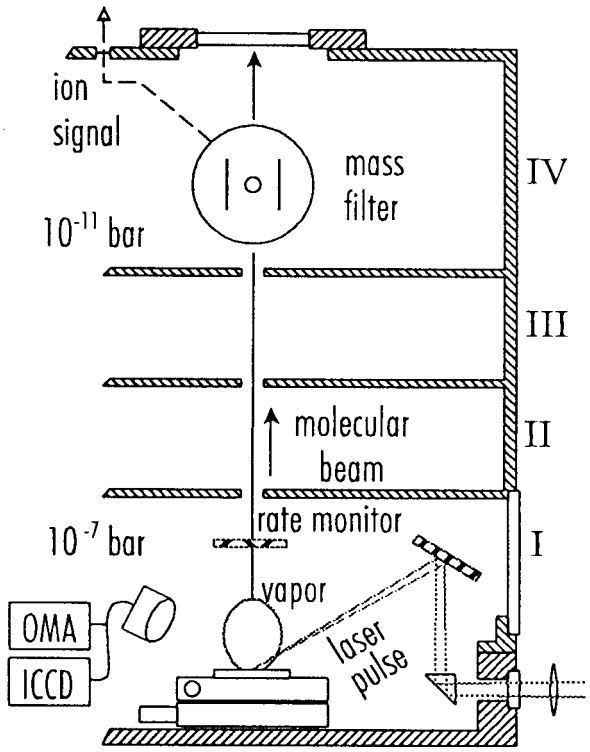


**Fig. 1** Schematic of LVMS apparatus, together with *in situ* deposition rate monitor and OMA, ICCD optical detectors.

- four differentially pumped vacuum stages. For continuous beam calibration experiments [e.g., see ref. 5, a chopping wheel (not shown) was positioned in stage III (see Fig. 1)].
- a quadrupole mass filter, positioned in stage IV with a cross-beam electron impact ionizer. The distance of the ionizer from the target was nominally 47.4 ± 0.3 cm (targets were repeatedly positioned within ±0.05 cm). This separation allowed for relatively unrestricted high-speed pumping in all stages; it also provided for a time delay (relative to the laser pulse onset) suitable for time-of-flight measurements with good mass and velocity discrimination.
- both digital (pulse counting) and analog multichannel detection of mass spectral ion intensity signals. Use of digital detection avoided the need to consider multiplier mass and species-type discrimination factors usually coupled with the measurement or use of ionization cross sections.
- optical multichannel analyzer (OMA) spectrometer for monitoring light emission over the range $\lambda$ = 185 nm to 1100 nm at successive times, with 5 ns time resolution. These data were used to reveal the presence of spectral emissions from vapor species that are usually indicative of the onset of laser–vapor plume interaction. By fitting the intensity-wavelength dependence to a Planck radiation function, the target hot spot temperature could be obtained, in addition to the cooling rate. These measurements were typically made simultaneously with deposition rate measurements.
- intensified charge-coupled device (ICCD) camera capable of 5 ns time resolution gating, which yielded data on the dimensions of the hot spot and relative temperatures. In addition, the onset of a visible laser-excited plume or the ejection of particulates could also be monitored with this device.

## APPROACH

The general experimental and data analysis approach is as follows, with the discussion giving emphasis to those aspects not described elsewhere.

### Laser-induced vaporization

In recent years we, and many others, have utilized laser materials interaction for the processing of thin films or coatings [13]. The usual requirement of a stoichiometric transport of target material to a substrate necessitates use of relatively short $\lambda$ photons with sufficiently high fluence (energy density $E$, J cm$^{-2}$) to produce a high energy (~50 eV) luminous plasma with nonthermal properties. With LVMS, avoiding the onset of any laser–plume interaction is desirable, in so far as possible. In general, this condition requires use of a relatively low fluence near the threshold for detectable vaporization. Use of longer $\lambda$ laser radiation (e.g., 1064 nm vs. 248 nm) also reduces the contribution of nonthermal interactions at the target. But, if the fluence is too far above threshold then inverse Bremstrahlung and other laser–vapor interactions can occur more readily at longer $\lambda$. The ideal fluence and $\lambda$ conditions are specific to each target material and, to a lesser extent, its prepared density and microstructure. With increasing fluence, the transition from thermal vaporization to plasma formation and ablation can readily be monitored with a fast-gated ICCD camera (as increased light emission) or with the deposition rate monitor (as markedly increased rate of deposition). The dependence of deposition (and hence vaporization) rate on laser fluence was generally determined in order to identify the threshold for a markedly increased dependence where the onset of a luminous plasma was noted. The pressures were determined from rate measurements, and LVMS experiments were usually carried out below the plasma onset fluence. The mass spectrometer signals also reveal plasma effects in the form of additional, faster time-of-arrival (TOA) profiles (see below) and an increased abundance of ions not formed by electron impact in the MS ionizer.

### Vapor expansion and beam formation

We have considered the vapor expansion-beam formation process in some detail elsewhere [14]. Monte-carlo [15,16], hydrodynamic flow [16], and chemical kinetic [5] models, together with ICCD imaging [17] and MS determination of velocity distributions [16], have indicated the essential features of this process. Basically, under the conditions used for LVMS, the vapor expands isentropically, and simple relationships exist between the pre- and post-expansion properties of temperature and pressure. The expansion to an effectively collisionless state is also sufficiently rapid (~100 ns) that the chemical composition of the pre-expansion vapor is essentially unchanged [5]. A collision-free vapor stream forms within a few mm of the target surface and is collimated to give a directed molecular beam by an aperture between stages I and II (see Fig. 1).

### Mass spectral analysis

The mass spectral analysis procedure is similar to that for KMS, as is the relationship between partial pressure ($p_i$) and the ion intensity ($I_i$) produced by electron impact of species $i$:

$$p_i \simeq k_i I_i T_s \quad , \tag{1}$$

where $T_s$ is the vapor temperature at the target prior to expansion and $k_i$ a constant that contains factors dependent on species identity. Ionizing electron energies of 26 ± 0.5 eV (corrected for the MS work function using known species appearance potentials) were generally used, with checks being made at lower energies for cases where species fragmentation may be significant. At this nominal energy, fragmentation interference was generally found to be insignificant (for expansion-cooled beams) and, from appearance potential curves and model considerations, ionization cross-sections were expected to be near their maximum values. Routine determinations of the MS intensity-time profiles (TOA) and, in some cases, appearance potential curves, were used to monitor the possible contribution of electron impact fragmentation to the MS-selected ion signals. In practice it is desirable to sum $I_i$ over the entire time-of-arrival peak of the molecular beam at the MS ionizer (i.e., $I_i$ becomes the area of the time-of-arrival thermal intensity-time profile after base-line subtraction). The constant $k_i$ can be expressed as

$$k_i = k / (\sigma_i S_i) \quad , \tag{2}$$

where $k$ is an instrument geometry/sensitivity constant valid for all species; $\sigma_i$ (discussed below) is the ionization cross-section; $S_i$ contains quadrupole and multiplier, together with hydrodynamic beam-forming, dependencies on molecular weight. $S_i$ is determined using a standard gas mixture, in the form of a hydrodynamic beam, as described elsewhere [18]. In contrast to KMS, where the vapor angular distribution is nominally $\cos\theta$, $k$ also depends on the exponent $n$ in the $\cos^n\theta$ distribution of the vapor plume, where $n$ is typically in the range $4 \le n \le 20$ for the laser spot size and vapor pressures used in the present studies.

Several independent approaches are used for $k$ determination. Materials with relatively well-established partial pressures may be used together with eqs. 1 and 2. For instance, we have used NaCl($\ell$), B($\ell$) (from BN), Si($\ell$) (from SiC), and C(s) for this purpose. A potentially more accurate approach, developed in the present study, is to determine total pressures from deposition rates, as discussed below, *in situ* with the mass spectrometric experiments. Thus, uncertainties associated with literature thermochemical data are avoided. In this study we compare results obtained by both approaches.

### Ionization cross-sections

The significance of ionization cross-sections ($\sigma$) to high-temperature mass spectrometry has recently been considered in detail elsewhere [19]. In the present study, $\sigma$'s for the elements were either those

measured by Freund *et al.* [20] or most often the calculated values of Mann [21]. In the absence of experimental values for the molecules encountered here we used a model described in detail elsewhere [22]. This predictive model has been shown to reproduce known experimental values, with the possible exception of one or two cases where autoionization, not accounted for by the model, may have been present. Notably, the model σ's for closed-shell electron configuration molecules are relatively low compared to other species or other estimates. We find, however, that such values are supported in these studies by equilibrium constant measurements, for example, for:

$$M + O_2 = MO + O,$$

where M = Mg, Ba, and by stoichiometric tests. For instance, from a stoichiometric (as confirmed by deposit analysis) vaporization of $BaTiO_3$, where BaO and TiO were the major MS-determined vapor species, we determined σ(BaO) = 1.7 ± 0.35 ($\times 10^{-16}$ cm$^2$) at 26 eV. The model value is calculated as $2.0 \pm 0.6 \times 10^{-16}$ cm$^2$. Summation of element σ's, used in some estimations (e.g., as in ref. 1), would give a value of $18.6 \times 10^{-16}$ cm$^2$.

The model is based on the viewpoint that heteronuclear high-temperature species generally are ionically rather than covalently bonded [23]. The model has the form

$$\sigma \simeq N/I_v \quad , \tag{3}$$

where $I_v$ is the vertical ionization potential, either measured by MS or calculated using a coulombic model [24]; $N$ is an *effective* number of electrons contributing to the ionization process. Values of $N$ are obtained from the ionic bond assignment where in $M^+ X^-$, for example, values of $N$ for $M^+$ or $X^-$ are taken from the isoelectronic elements whose $N$'s are obtained from the above equation using known σ's and $I_v$'s.

## Deposition rates

Deposition rate measurements were used to obtain values of $n$ for the $\cos n\theta$ distribution of species in the expanded vapor and also to obtain values of total pressure (i.e., the aggregate of partial pressures). $\cos^n\theta$ distributions have been confirmed by two approaches. In addition, the values (given below) obtained by both approaches are consistent with values obtained earlier from a hydrodynamic model, from ICCD imaging (e.g., see ref. 16) and from MS-stage tilting angular distribution experiments. The two principal approaches used were: (a) we utilized the rate monitor (RM) *in situ* with the MS system. The RM (mounted on a 22-cm lever arm) was moved in an arc parallel to the plane of the target surface. By fitting the data to a $\cos^p\theta$ function, values of $p$ were obtained, as shown by the example in Fig. 2. It can be shown that for this parallel RM system geometry, values of n, appropriate to an ideal detector positioned on a spherical surface, are given by: $n = p - 3$; *(b)* a spatially resolved optical interference film thickness measurement was made across the deposited film [25]. The film deposition and RM geometries are equivalent, and similar results were obtained with both approaches.

Determination of total pressure ($P_t$) from deposition rate is well known for Knudsen effusion conditions. However, to our knowledge, this approach has not previously been used under hydrodynamic flow conditions, for which we derive the following relationship:

$$P_t = 10^{-6}\left(\frac{R\left(\ell^2 + r^2\right)\pi\rho}{f\Delta t A}\left[\frac{2\pi R_g T_s}{M}\right]^{0.5}\right)\left\{\frac{2}{n+1}\right\}H \tag{4}$$

where $P_t$ is in units of bar (= $10^5$ Nm$^{-2}$); $R$ is the (nominal) film thickness deposition rate in cm s$^{-1}$, calculated from the rate monitor scale reading given in Å (1Å = $10^{-10}$ m) and referenced to the total laboratory accumulation time; $f$ is the laser repetition rate in Hz (s$^{-1}$), typically 20 Hz—note that $R/f\Delta t$ is the actual thickness deposition rate per laser pulse; A is the measured hot spot area (cm2); $\ell$ is the distance

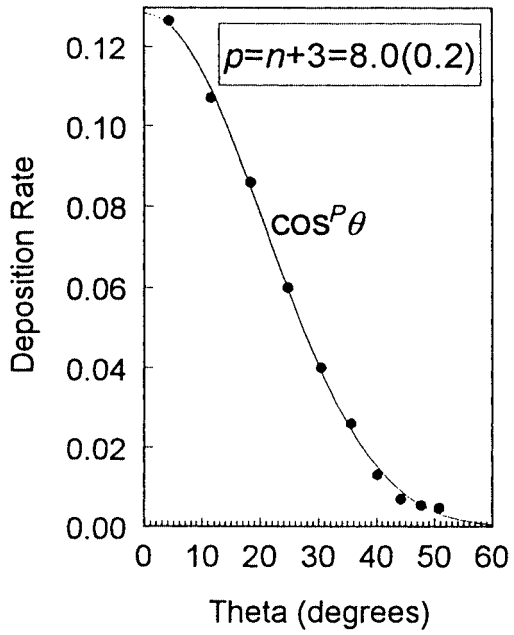


**Fig. 2** Angular dependence of graphite deposition rate (symbols) fitted to a $\cos^p\theta$ ($n = p - 3$) dependence (curve).

(cm) from target to monitor, typically 3 cm here; r is the radius of the exposed area of the rate monitor crystal (cm), typically 0.4 cm; $\Delta t$ is the measured effective hot spot time (s), typically 25 ns; ρ is the density (gm $cm^{-3}$) of the film (a nominal value used by the rate monitor to convert accumulated mass to thickness); $M$ is the average gm-molecular weight of the depositing species; $R_g$ is the gas constant (~$8.314 \times 10^7$ erg $K^{-1}$ $mol^{-1}$)—the factor $10^{-6}$ has the units bar $dyne^{-1}$ $cm^2$ (1 dyne $cm^{-2}$ = 0.1 Pa), to convert pressure from cgs units; $H = (1 - 0.18)^{-1}$ $(2\pi/e)^{-0.5}$ and contains factors for relatively small hydrodynamic back-scattering [9] and beam-intensifying [26] effects.

It has been shown experimentally (see discussion in ref. 30) and also by model calculations that thermalization and melting occur on a time-scale shorter than 1 ns. Similarly, at the end of the laser pulse, cooling to a temperature level where the vaporization rate is negligible can be expected to occur within a few ns. In the present study, we monitored the thermal transient using the OMA and ICCD detectors and the $T$ vs. $t$ response, $\Delta t$, was close to that of the laser pulse duration itself (~20 ns). The laser pulse was comprised of three overlapping short pulses, effectively giving rise to a near-top-hat profile. For the materials considered here and the Nd:YAG laser used, we determined $\Delta t = 25 \pm 5$ ns to be the time that the hot spot was at its effective vaporizing temperature.

Values of $P_t$ obtained by use of eq. 4 are considered to be accurate to ±25%. Contributing uncertainties [±percent], include $A$[10], $R$[10], $n$[5], $M$[5], $\Delta t$ [20]. Other uncertainty factors, including $T$ [1], are minimal. It is also noteworthy that the influence of σ (as $\sigma^{-0.5}$), in the determination of $M^{0.5}$, is significantly less than for the $P_t$ method based on, for example, eq. 1, where $p_i \propto \sigma_i^{-1}$. Overall, however, the uncertainties associated with pressure determinations based on eqs. 1 and 4 are similar.

## Temperature determinations

In our initial LVMS studies [4] it was not possible to measure temperature ($T_s$) directly on the short time scale of the laser pulse duration (~20 ns). Several indirect approaches were developed and are still used for cases where a direct approach is not possible. To reiterate, the indirect approaches are: (a) comparison of measured (LVMS) with known equilibrium reaction constants ($K_p$) e.g. for $C_5/C_3$ over C(s) and $Si_2$/Si over Si(ℓ); (b) use of pressures obtained from the deposition rate data, together with literature

*P-T* data; and (c) use of an established [5] direct relationship between $T_s$ and beam temperature ($T_b$) obtained from velocity distributions or from time-of-arrival (TOA) versus $M^{1/2}$ dependancies. These approaches lead to temperatures ($T_s$) that appear to be accurate to better than about 3%.

In this study we have also used a more direct approach (see Apparatus section) based on the Planck radiation expression:

$$I(\lambda, T_s) = A\lambda^{-5} / \left[ e^{\frac{c_2}{\lambda T_s}} - 1 \right] \tag{5}$$

where $A$ is a fitted intensity ($I$) scale factor, and contains factors for both emissivity and optical losses; $c_2$ is the second radiation constant ( = $1.438786 \times 10^7$ nm·K); $A$ and $T_s$ are the nonlinear fitting parameters. Data obtained by this approach are believed to be accurate to ±1%, depending on the material system. Statistical uncertainties are typically only ±5 K. Additional uncertainty arises from the presence of a temperature distribution across the hot spot. The observed temperature is then an effective ("average") value, weighted towards the maximum. As the observed vaporization time is also an effective average, uncertainties arising from the distribution of temperature and rate with the thermal pulse time and across the hot spot tend to be self-compensating.

## RESULTS AND DISCUSSION

Table 1 summarizes representative results relating to total pressure determinations. Additional results and details are given in the figures and discussion. An overall excellent agreement between pressures obtained by the LVMS and rate methods is evident in Table 1. Good agreement is also found with the selected extrapolated literature values (i.e., certain, but not all, literature values show good agreement). These results rule out the presence of any significant, unaccounted for, higher-molecular-weight cluster species, as that case would lead to much higher calculated (with noncluster M-values) $P_t$ - rate pressures than those determined by LVMS or from literature thermodynamic functions.

**Table 1** Total pressures.

| System | Temperature | Total pressure (bar = $10^5$ $Nm^{-2}$) | | | | |
|---|---|---|---|---|---|---|
| | K | From rate[e] | n[d] | M[h] | LVMS[e] | Literature |
| C(s) | 4100[c] | 1.8 | 5 | 33 | 1.2[f],1.8[g] | 1.8(2)[a], 1.1(11), |
| | 4109 | 2.1 | 11.7 | | | 1.1(12), 1.0(1), |
| | 3602 | 0.13 | " | | | all at 4100 K; |
| | 4237 | 5.6 | " | | | see also Fig. 4 |
| SiC→Si(ℓ) C(s) | 3057 | 0.15 | 11.7 | 31 | | 0.16(1) |
| | 3300[c] | 1.1 | 3.0 | 31 | 0.6[f], 0.9[g] | 1.2(1) |
| $Al_2O_3$(ℓ) | 3500[c] | 0.15 | 4[b] | 27 | 0.08[f], 0.13[g] | 0.08(1); 0.09(2) |
| | 3900[c] | – | | | 0.6[f], 0.9[g] | 0.9(1); 0.6(2) |
| | 4300 | 3.9 | 4.5 | 26 | | 3.4(1); 4.0(2) |
| | 4332 | 4.6 | | | | 4.2(1); 4.5(2) |
| | 4719 | 20.7 | | | | 14(1); 19(2) |

[a]Corrected for $C_5$ (see text).
[b]Estimated from $n$ vs. spot diameter correlation (±10%).
[c]From TOA data (all other $T$'s from Planck method).
[d]Uncertainty ±6%; for $n$ = 11.7, spot area = $1.13 \times 10^{-2}$ $cm^2$, for 3,4,5, = $4.9 \times 10^{-3}$ $cm^2$, and for 4.5, = $1.3 \times 10^{-3}$ $cm^2$.
[e]Uncertainty ±25% for rate and LVMS.
[f]Based on $P_{C_3}$ from ref. 1.
[g]Based on revised $P_{C_3}$ = 1.3 bar, from Table 2.
[h]Average value for temperature range, based primarily on LVMS measurements.

An example of temperature measurement using the Planck radiation approach is given in Fig. 3. Based on the good agreement between observed intensities and the Planck curve over a wide range of λ, we assume a constant emissivity ("grey body" behavior). For graphite, and the other materials studied, we find that the cooling rate follows the time dependence of the laser pulse to a good approximation.

### C (graphite)

Graphite has advantages as a reference or calibration system for LVMS as it remains solid up to relatively high pressures and has been extensively studied at lower temperatures. Nevertheless, the two main critically evaluated reference tables JANAF [1] and IVTANTHERMO [2] still have small but notable differences, as we discussed in our original work on this system [4]. The latter compilation [2] is more recent, and the spectroscopically based entropy functions are given higher precision. However, the enthalpy data of both compilations are based essentially on the same experimental data, with JANAF favoring the results obtained by a second law thermodynamic approach (i.e., relative $P$ vs $T$ data analysis) and IVTANTHERMO favoring the third law approach (i.e., absolute $P$ data analysis). We find that the LVMS-determined partial pressures (LVMS + Rate column in Table 2) are consistent within the stated literature uncertainties, with both the JANAF and IVTANTHERMO values. The latter tables appear to significantly overemphasize the partial pressure of $C_5$—using our value for this species reduces the IVTANTHERMO total pressure to a value in good agreement with the present work. Using our rate-determined $P_t$ value to obtain $k$ for the LVMS data yields $C_n$ partial and total pressures that are the most consistent with the available literature results. These pressures are also consistent with the temperatures obtained from *both* the indirect and direct approaches, provided the JANAF and IVTANTHERMO $P_i$ ratios ($C_5/C_3$) are adjusted for the σ's used in Table 2. Thus, for instance, the JANAF values of $C_5/C_3$ are increased by a factor of 1.8. In addition, use of the LVMS-rate graphite pressures for $k$ determination leads to much better agreement among $P_t$'s obtained by the rate and LVMS methods, separately, and with the literature values for each of the systems studied.

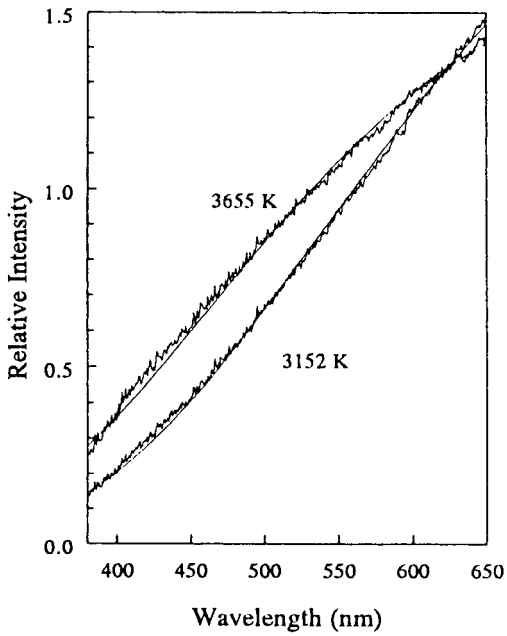


**Fig. 3** Emission intensity vs. wavelength dependencies for laser-heated graphite, with two different fluences and an observation time of 100 ns; smooth curves are for Planck radiation model with $T_s$ = 3655 K and 3152 ± 6 K.

**Table 2** C(s) Partial pressures (bar = $10^5$ $Nm^{-2}$), at 4100 K.

| Species | LVMS[a] | | | | LVMS+rate[f] | Literature | |
|---|---|---|---|---|---|---|---|
| | $I\Delta t$ (counts) | $S$ | $\sigma$ [b] ($\times 10^{-16}$ $cm^2$) | $P_i$ | $P_i$ (1) | $P_i$(1)[d] | $P_i$(2)[e] |
| $C_1$ | 1100 | 0.77 | 1.6 | 0.082 | 0.12 | 0.104 | 0.103 |
| $C_2$ | 3750 | 0.84 | 2.4 | 0.170 | 0.26 | 0.152 | 0.182 |
| $C_3$ | 23420 | 0.88 | 3.0 | (0.83) | 1.3 | 0.83 | 1.45 |
| $C_4$ | 940 | 0.94 | 3.6 | 0.025 | 0.04 | 0.11 | 0.050 |
| $C_5$ | 1860 | 0.94 | 4.5 | 0.040 | 0.07 | 0.023 | 0.29 |
| $C_6$ | 230 | 0.93 | 5.1 | 0.004 | 0.006 | - | -[c] |
| $C_7$ | 560 | 0.92 | 5.8 | 0.010 | 0.015 | - | - |
| $C_8$ | 35 | 0.88 | 6.5 | 0.0005 | 0.0007 | - | - |
| $C_9$ | 230 | 0.80 | 7.2 | 0.003 | 0.0045 | | |

[a]LVMS parameters: $k = 2.25 \times 10^{-8}$ atm $K^{-1}$ $counts^{-1}$ $t^{-1}$ (analog-to-digital averager), where $\sigma$ units of $10^{-16}$ $cm^2$ are set to unity here and elsewhere; $n = 5$; $\lambda = 532$ nm; $E = 0.9$ J $cm^{-2}$.
[b]$\sigma$'s; $C_1$ (Mann), $C_2 - C_4$ (models), $C_5 - C_9$ (est. from $C_1 - C_4$, $C_{60}$ )
[c]For $C_6 - C_9$, $\Sigma p_i \sim 0.02$ bar.
[d]Uncertainty = factor of 4.
[e]Uncertainty = factor of 3.
[f]From $P_t$ rate (Table 1), $k = 3.37 \times 10^{-8}$ (units, see a.).

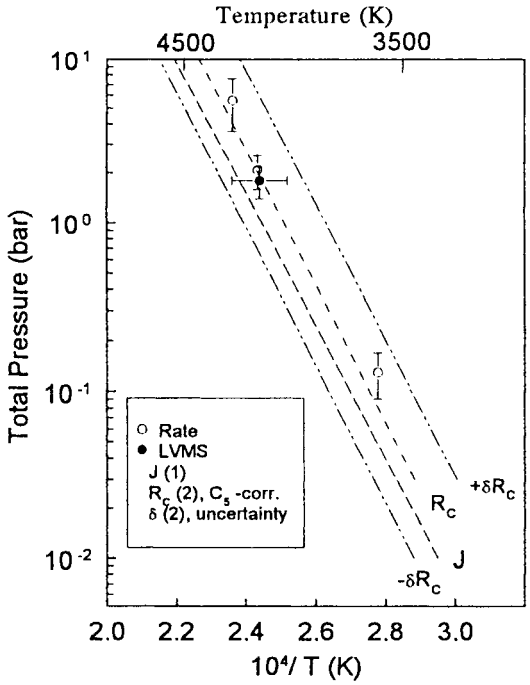


**Fig. 4** Comparison of graphite LVMS and rate *P-T* data (symbols) with literature thermochemical values (curves). Size of data symbols for present work indicates experimental uncertainty.

Values of $n$ (for $\cos^n\theta$) used for the pressure determinations based on eq. 4 are given in Table 1, and Fig. 2, above, shows a typical result, obtained using the *in situ* rate monitor. The partial and total pressure data are compared with evaluated literature values in Fig. 4 and in Tables 1 and 2.

## SiC

Using similar procedures to those for graphite, *P-T* data were obtained as shown in Table 3 and Fig. 5. The indirect temperature (3300 K) was obtained by comparing $T_b$ (from analysis of TOA data)

**Table 3** SiC($\ell$,s) partial pressures (bar = $10^5$ Nm$^{-2}$) at 3300 K.

| | LVMS[a] | | | | LVMS[c] | Literature[d] | |
|---|---|---|---|---|---|---|---|
| Species | $I\Delta t$ (counts) | S | σ ($\times 10^{-16}$ cm$^2$) | Pi | Pi | Pi(1) | Pi(2) |
| Si | 100 | 0.88 | 5.1[b] | 0.44 | 0.66 | 0.4 | 0.45 |
| $Si_2$ | 5 | 0.95 | 5 | 0.02 | 0.03 | 0.02 | 0.06 |
| SiC | 4 | 0.9 | 4.0 | 0.02 | 0.03 | 0.003 | 0.004 |
| $Si_2C$ | 8 | 0.9 | 4.0 | 0.04 | 0.06 | 0.23 | 0.94 |
| $SiC_2$ | 13 | 0.9 | 3.3 | 0.08 | 0.12 | 0.6 | 1.55 |

[a]$k = 6.0 \times 10^{-6}$ atm K$^{-1}$ counts$^{-1}$ t$^{-1}$ (multichannel counter), based on $P_{C_3}$ (1); λ = 532 nm, E = 0.9 J cm$^{-2}$.
[b]$\sigma_{Si}$ = 6.6 (20),= 5.1 (21).
[c]Recommended values using $k = 9.0 \times 10^{-6}$ atm K$^{-1}$ counts$^{-1}$ t$^{-1}$, based on revised $P_{C_3}$ (see Table 2).
[d]For case SiC (cr,$\ell$).

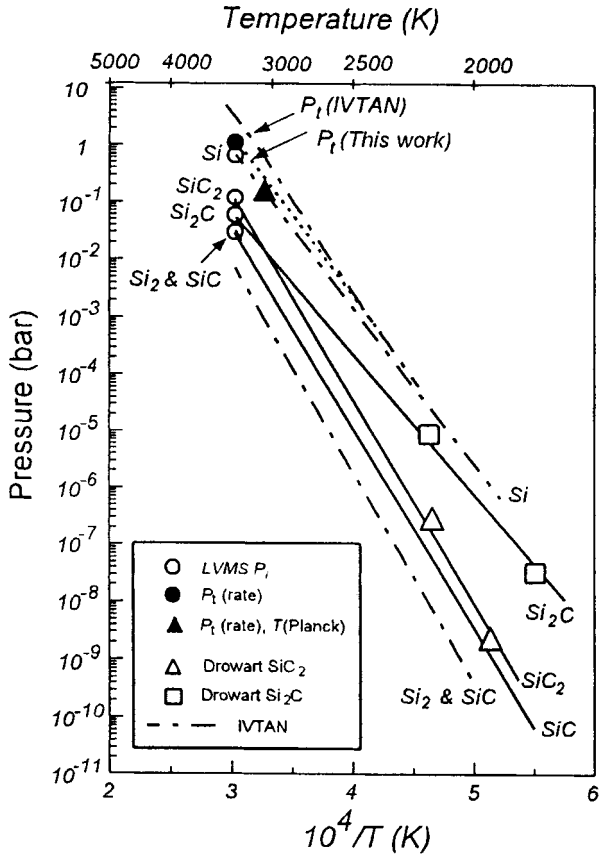


**Fig. 5** Comparison of SiC LVMS $P_t$ and deposition rate $P_t$ vs $T$ data with extrapolated selected literature values. Drowart [28]; Si, $Si_2$ [2]; SiC, IVTAN [2].

with that for C, where $T_s$(C) is known [i.e., $T_s$(SiC) = $T_s$(C) · $T_b$(SiC)/$T_b$(C)]. As was discussed in earlier studies [5], the shapes of the TOA profiles and their dependence on $M^{0.5}$ together with appearance potential curve analysis, were used to verify the ion-to-precursor assignments. Note in Table 3 and Fig. 5 that the partial pressures of SiC, $SiC_2$, and $Si_2C$ differ significantly from the extrapolated lower pressure evaluated literature data. We also note that the present results differ from our earlier preliminary ones, owing to an incorrect assignment of hydrocarbon impurities to $C_1$ and $C_2$ [27]. For $SiC_2$ and $Si_2C$, the lower temperature data of Drowart and DeMaria [28], adjusted for our model σ's, are consistent with our results at higher temperatures.

### $Al_2O_3$

$Al_2O_3$ is a relatively well-studied system, and the critically evaluated literature [1,2] may be used to further test the LVMS method and also the evaluation procedures. Because the target maintains a constant deposition rate over time (which was not always the case for other materials), this material is useful as a calibrant (e.g., for determining *k* for use in LVMS experiments with other materials). Tables 1 and 4 show very good agreement between the present results and the evaluated literature, with the main differences being related to use of different σ's.

### $ZrO_2$–7% $Y_2O_3$

Relative abundances of ZrO and $ZrO_2$ were obtained by LVMS and the results used to calculate *M*, which, combined with deposition rate measurements, yielded values of $P_t$. Temperatures were obtained by the Planck radiation method. The results are compared with extrapolated literature data in Fig. 6. Upon heating under vacuum, $ZrO_2$ changes color, first to a gray then to a black form, due to preferential loss of oxygen. The two data sets in Fig. 6 represent the initial fully oxidized $ZrO_2$ form and a reduced form with approximate composition $ZrO_{1.75}$. For the selected literature curves (extrapolated from studies over solid $ZrO_2$) remarkable agreement is found with the IVTANTHERMO tables [2] for the $ZrO_2$ form and with the data of Hoch *et. al.* [29] for the reduced system. The small contribution of volatiles from $Y_2O_3$ can be neglected for these comparisons.

### $Y_2O_3$

Figure 7 compares data obtained by the rate method with extrapolated literature curves. Based on the lower temperature literature MS observations [31] and bond energy arguments we expect YO and O as

**Table 4** $Al_2O_3$ partial pressures (bar = $10^5$ $Nm^{-2}$) at (A) 3500 K and (B) 3900 K.

| Species | A | | | | | B | | | |
|---|---|---|---|---|---|---|---|---|---|
| | LVMS[a] | | | Literature | | LVMS[a] | | Literature | |
| | $I\Delta t$ (counts) | $S$ | σ ($\times 10^{-16}$ $cm^2$) | $P_i$ | $P_i$(2) | $I\Delta t$ (counts) | $P_i$ | $P_i$ (1) | $P_i$(2) |
| Al | 3 | 0.83 | 6.1[b] | 0.018 | 0.014 | 22 | 0.10 | 0.10 | 0.10 |
| O | – | 0.9 | 0.7 | | 0.019 | 9.4 | 0.54 | 0.24 | 0.28 |
| AlO | – | 0.96 | 1.2 | | 0.020 | 4.8 | 0.15 | 0.16 | 0.18 |
| $Al_2O$ | – | 0.96 | 6.1 | | 0.006 | 5.0 | 0.03 | 0.05 | 0.07 |
| | | | | | | $P_t$ = | 0.82 | 0.55 | 0.63 |

[a] $k = 9.0 \times 10^{-6}$ atm $K^{-1}$ $counts^{-1}$ $t^{-1}$ (from $p_c$, see Table 2), λ = 532 nm.
[b] 9.6 (20).

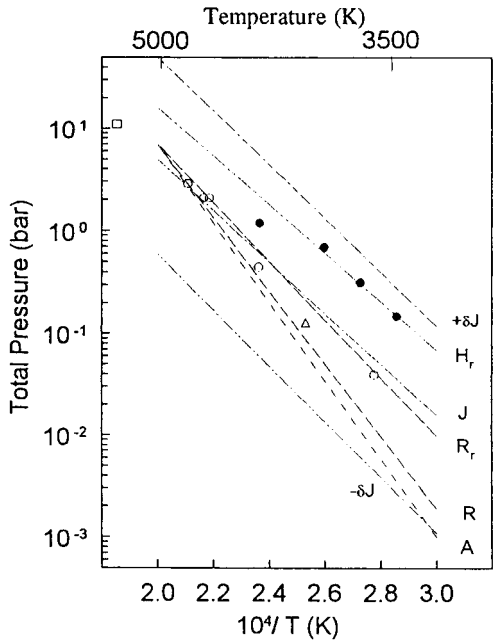


**Fig. 6** Comparison of $ZrO_2$ – 7%$Y_2O_3$ $P_t$ vs. $T$ data with extrapolated literature values (curves). Open symbols are for unreduced (i.e., initial) material, and closed symbols are for the partially reduced system (see text). $P_t$ obatined using $n$ = 11.7, $M$ = 92, and $P(ZrO)/P(ZrO_2)$ = 0.5 (LVMS). Data uncertainty limits are similar to those indicated in Figs. 4 and 7. Curve A, extrapolation of Ackerman *et al*. [30] data for vaporization to $ZrO_2$ (g); curve R [2]; curve J [1], ± δJ uncertainty; curve $H_r$ extrapolation of Hoch *et al*. [29] $ZrO_2$(s) + Zr(s) system; curve $R_r$ calculated from [2] for $ZrO_2$ ($\ell$) + Zr($\ell$) system.

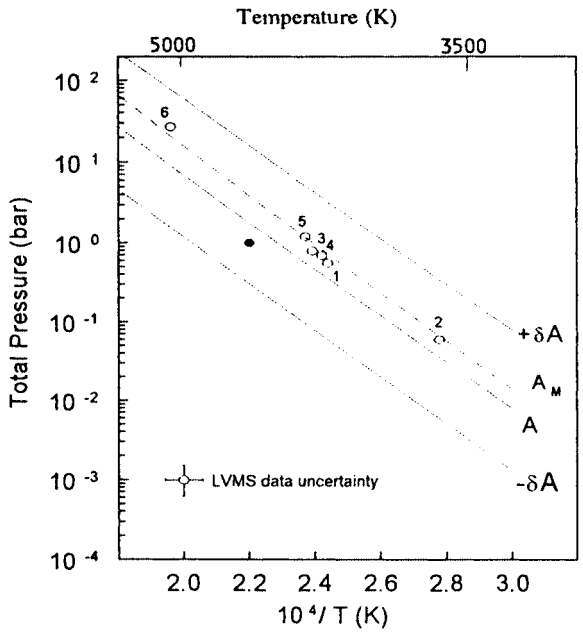


**Fig. 7** Comparison of $Y_2O_3$ $P_t$ vs. $T$ data with extrapolated literature values (curves) $n$ = 11.7, $M$ = 90. Data points (open circles) are numbered in chronological order. Curve A is extrapolated from solid-phase data of Ackerman *et al*. [31] with an estimated enthalpy of melting; ±δA are uncertainties of [31]; curve $A_M$ is extrapolated from Ames *et al*. [32]; filled circle point is 1 bar ($10^5$ $Nm^{-2}$) $P$ at $T$ cited by Schick [33].

the significant vapor species, from which $M$ may be calculated. Good agreement is found with the extrapolated data of Ackermann *et. al.* [31] and particularly that of Ames *et. al.* [32].

## SUMMARY AND CONCLUSIONS

Previous limitations associated with the application of laser vaporization mass spectrometry to thermochemical studies at very high temperatures have been resolved to the extent that new, more accurate vapor pressure and related thermodynamic properties can now be determined. In particular, the measurement of time-resolved thermal emission intensities over a wide range of wavelength has allowed for direct temperature determinations. Significant improvements in the ease of measurement, and in data accuracy, have been made for the determination of total and partial pressures. A key development in this respect has been the use of *in situ* deposition rate measurements, concomitant with the mass spectrometric and temperature measurements. Also, the ability to sweep the position of the rate monitor across the vapor plume now allows for *in situ* measurement of the $\cos^n\theta$ spatial distribution which can differ appreciably ($n \sim 4$ to 12 or more, typical) relative to the usual effusive behavior where $n = 1$. With a knowledge of this distribution, one can readily relate the measured deposition rate to the vaporization rate of the sample. Then the classical Hertz–Langmuir gas–kinetic relationship, modified for hydrodynamic conditions, can be used to determine pressure from vaporization rate provided the vapor molecular weight ($M$) is known, where $M$ is typically an abundance-weighted average of the various species present. To obtain $M$, the MS analysis of ions must yield the correct molecular precursors and their relative abundance. The precursor assignment is greatly enhanced by the use of velocity or time-of-arrival information, readily obtained by LVMS. Also, the order-of-magnitude cooling associated with the vapor expansion process appears, in most cases, to reduce the degree of electron impact fragmentation normally present in high-temperature (KMS) beams.

The LVMS technique should be applicable to most inorganic materials with the following limitations. The material must be absorbing (even if only to a limited extent) at the available laser wavelength, although materials with a small extinction coefficient (e.g., $Al_2O_3$) can be heated by short-pulse lasers. Fortunately, laser wavelengths are available over a wide spectral range. The total pressure range appears to be limited typically to about 0.01 to 10 bar for short-pulse lasers and to about $10^{-6}$ to $10^{-4}$ bar for long-pulse lasers. The useful temperature range appears to be limited to about 3000 to 5500 K, depending on the system, and to where Planck radiation behavior can be used to measure temperature. The range can be expanded if indirect temperature measurements, based on velocity distribution analysis and known chemical equilibria, are used. We can expect the accuracy of the LVMS method to decrease at some upper level temperature and pressure. A limiting condition can be expected as light absorption (and emission) by the high density vapor or ionization (expect low $T_s$ determination) becomes important. Also, onset of cluster formation during expansion would affect $M$ determination for $P$-rate, leading to a high $P_t$ determination.

With respect to the systems considered here, it appears that new critical evaluations may be warranted for the candidate reference systems of C and $Al_2O_3$. Likewise, for the other systems studied, the partial and total pressures obtained by LVMS can be used to refine existing (estimated), or to generate new, thermodynamic functions and bond dissociation energies. More reliable estimates of the critical point $T,P$ should also be possible using the present data. We note that the strong preference given to third law versus second law critical evaluations of the lower temperature vaporization data (e.g., see ref. 2) may not always be warranted. From the LVMS results obtained to date, it appears that the extrapolated KMS data, where available, are sometimes more reliable than one might expect, given the dependence on estimated enthalpies of melting and many other thermal and spectroscopic parameters.

A discussion of the need for measurements in the "kilodegree" temperature range, given by Beckett in 1967 [34], is still pertinent. Similarly, in the context of predictions of $T, P$ conditions under which metal dimers could be seen by high-temperature mass spectrometry Verhaegen *et al.* [35] noted in 1962, "...conventional mass spectrometric techniques (KMS) will have to be greatly improved to per-

mit one either to reach the temperatures (~4000 K) or to handle the pressures (~1 bar) in the extreme cases". The LVMS technique appears to meet this need.

## REFERENCES


1. M. W. Chase, Jr., C. A. Davies, J. R. Downey, Jr., D. J. Frurip, R. A. McDonald, A. N. Syverud. *JANAF Thermochemical Tables*, 3rd ed., *J. Phys. Chem. Ref. Data* **14**, Suppl. No. 1, ACS, Washington, DC (1985).
2. L. V. Gurvich, I. V. Veyts, C. B. Alcock. *Thermochemical Properties of Individual Substances*, 4th ed., Vols. 1–3, Hemisphere Pub. Corp. New York (1989). Also see original Russian editions *loc. cit.*, and *NIST Special Database 5*, "IVTANTHERMO" (L.V. Gurvich, V. S. Iorish, D. V. Chekhovsioi, V. S. Yungman. CRC Press, Boca Raton, Florida, 1993), a program that incorporates the above tabulations to ~1992, and can compute multicomponent equilibria based on the database.
3. J. W. Hastie, D. W. Bonnell, P. K. Schenck. *High Temp. High Press* **20**, 73 (1988).
4. J. W. Hastie, D. W. Bonnell, P. K. Schenck. *High Temp. Sci*. **25**, 117 (1988).
5. J. W. Hastie, D. W. Bonnell, A. J. Paul, J. Yeheskel, P. K. Schenck. *High Temp. Sci*. **33**, 135 (1995).
6. J. W. Hastie. *High Temperature Vapors-Science and Technology*, Academic Press, New York (1975).
7. J. W. Hastie, A. J. Paul, D. W. Bonnell, P. K. Schenck. *High Temperature Synthesis of Materials*, ACS Symposium Series 681, D. Gruen and M. Serio (Eds.), p. 39, ACS, Washington, DC (1998).
8. R. W. Ohse, J. F. Babelot, C. Cercignani, P. R. Kinsman, K. A. Long, J. Magill, A. Scotti. In *Proc. 10th Materials Research Symp. Characterization of High Temperature Vapors and Gases*, J. W. Hastie (Ed.), p. 83, NBS SP 561, NTIS, Washington, DC (1979).
9. D. Olander. Page 411 in *Materials Chemistry at High Temperatures 2*, J. W. Hastie, (Ed.), Humana Press, New Jersey (1990).
10. a) R. L. Baker, M. A. Covington, G. M. Rosenblatt. Page 143 in *High Temp. Materials II*, Z. A. Munir, D. Cubicciotti (Eds.), Electrochem. Soc., Pennington, New Jersey (1983); b) M. A. Covington, G. N. Liu, K. A. Lincoln. *AIAA Journal*, **15**, 1174 (1977).
11. J. H. Lundell and R. R. Dickey. "Response of Heat-Shield Materials to Intense Laser Radiation," p. 193, *AIAA 16th Aerospace Sciences Meeting*, Huntsville, Alabama, Jan. 16, AIAA, New York (1978).
12. *Phase Diagrams for Ceramists*, a continuing series published by The American Ceramic Society, Westerville, Ohio.
13. D. B. Chrisey and G. K. Hubler (Eds.). *Pulsed Laser Deposition of Thin Films*, Wiley, New York (1994).
14. A. J. Paul, P. K. Schenck, D. W. Bonnell, J. W. Hastie. In *Proc. MRS Symp. Film Synthesis and Growth Using Energetic Beams*, **388**, 45, MRS, Warrendale, Pennsylvania (1995).
15. A. Ranjin, S. Sinha, P. K. Ghosh, J. W. Hastie, D. W. Bonnell, A. J. Paul, P. K. Schenck. *J. Chem. Phys. Lett*. **277**, 545 (1977).
16. J. Paul, J. W. Hastie, P. K. Schenck, D. W. Bonnell, M. D. Vaudin. *Proc. MRS Symp.* Vol. 526, p. 243, MRS, Warrendale, Pennsylvania (1998).
17. P. K. Schenck, J. W. Hastie, A. J. Paul, D. W. Bonnell. *Opt. Eng*. **35**, 3199 (1996).
18. D. W. Bonnell and J. W. Hastie. In "Characterization of High Temperature Vapors and Gases," NBS SP 561, **1**, 357 (1979).
19. J. Drowart, C. Chatillon, J. W. Hastie, D. W. Bonnell. "High Temperature Mass Spectrometry: Accuracy of the Method and Influence of Ionization Cross Sections," *Pure Appl. Chem.* (2001), to be published.
20. R. S. Freund, R. C. Wetzel, R. J. Shul, T. R. Hayes. *Phys. Rev. A*, **41**, 3575 (1990).

21. J. B. Mann, Page 814 in *Recent Developments in Mass Spectrometry*, K. Ogata and T. Hayakawa (Eds.), Univ. Park Press, London (1969). See also ref. 19.
22. J. W. Hastie. "A Model for Ionization Cross Sections of High Temperature Molecules," to be published (2000).
23. J. W. Hastie and J. L. Margrave. *J. Phys. Chem*. **73**, 1105 (1969).
24. J. W. Hastie and J. L. Margrave. *Fluorine Chem. Rev*. **2**, 77 (1968).
25. P. K. Schenck, unpublished observations (2000).
26. a) K. D. Carlson, P. W. Gilles and R. J. Thorn, *J. Chem. Phys*. **38**, 2725 (1963); b) F. Tehranian, *The Kinetics of Laser Pulse Vaporization of Uranium Carbide by Mass Spectrometry*, (LBL-15982 Univ. Calif., Berkeley, CA, 1982).
27. D. W. Bonnell, P. K. Schenck, J. W. Hastie, M. Joseph. *Proc. Electr. Chem. Soc. Symp. High Temp. Chem*, ECS, Pennington, New Jersey (1990).
28. J. Drowart and G. DeMaria. *Silicon Carbide*, J. R. O'Conner and J. Smiltens. (Eds.), pp. 16–23, Pergamon, New York (1960).
29. M. Hoch, M. Nakata, H. L. Johnston. *J. Amer. Chem. Soc*. **76**, 2651 (1954).
30. R. J. Ackermann, E. G. Rauh, C. A. Alexander. *High Temp. Science* **7**, 304 (1975).
31. R. J. Ackermann, E. G. Rauh, R. J. Thorn. *J. Chem. Phys*. **40**, 883 (1964).
32. L. L. Ames, P. N. Walsh, and O. White. *J. Phys. Chem*. **71**, 2707 (1967).
33. H. L. Schick. *Thermodynamics of Certain Refractory Compounds*, Vol 1, Academic Press, New York (1966).
34. W. Beckett. *The Characterization of High Temperature Vapors*, J. L. Margrave (Ed.), p. 3, Wiley, New York (1967).
35. G. Verhaegen, F. E. Stafford, P. Goldfinger, M. Ackerman. *Trans. Far. Soc*. **58**, 1926 (1962).